Transition wavelengths and unresolved transition array statistics of ions with $Z = 72 - 89$

D. Kilbane

School of Physics, University College Dublin, Belfield, Dublin 4, Ireland

E-mail: Deirdre.Kilbane@ucd.ie

Abstract. Potential extreme ultraviolet and soft X-ray radiation sources have been identified, using the flexible atomic code (FAC), as emission peaks arising from 4d - 4f and 4p - 4d transitions in Pd-like to Rb-like ions of hafnium through actinium. The effects of configuration interaction are investigated and for increasing nuclear charge, these strong emitters are seen to separate and move to shorter wavelength. Each source is characterized using the unresolved transition array model. They are proposed to complement the currently used nitrogen and argon sources in the "water window", and as possible successors to tin in next generation lithography.

PACS numbers: 31.10.+z, 32.30.Jc, 32.70.-n, 32.80.Aa

1. Introduction

The success of extreme ultraviolet lithography (EUVL) hinges on the ability to identify powerful radiation sources at 13.5 nm, a wavelength at which molybdenum / silicon mirrors are highly reflective [1–4]. To date, both tin and xenon laser produced plasmas (LPPs) and discharge plasmas are the sources of choice at this wavelength: Sn^{8+} - Sn^{13+} emission due to 4d - 4f and 4p - 4d transitions and Xe^{10+} emission due to 4d - 5p transitions [1, 4–8]. Many recent research efforts have concentrated on investigating next generation lithographic sources at shorter wavelengths e.g. gadolinium and terbium at 6.75 nm [9–13]. In [14], extreme ultraviolet (EUV) and soft X-ray (SXR) sources were identified at numerous wavelengths with the prospect of being used in the event of a highly reflective mirror becoming available at any of these wavelengths.

Moving to shorter wavelengths, further into the SXR region, we enter what is known as the "water window" ($2.3-4.4$ nm), where live biological sampling is desirable [15, 16]. Current sources in this region are strong quasi-monochromatic emission at $\lambda = 2.879$ nm and $\lambda = 2.478$ nm wavelengths arising from $1s^2$ - 1s 2p in N^{5+} and 1s - 2p in N^{6+} respectively, and broadband emission between $\lambda = 2-4$ nm from argon gas targets [15]. Quasi-monochromatic sources are suitable for biological imaging using diffractive optics while broadband emission sources can be used for contact microscopy. The development of compact, high repetition rate, table top SXR sources using these gas puff targets, which have the advantage of being debris free, provide much needed laboratory *in situ* alternatives to free electron lasers and synchrotrons and can be used in numerous experiments, e.g. microscopy, spectroscopy and metrology.

It is proposed that the sources identified in this work would be generated in laser produced plasmas (LPPs), where a solid target is irradiated with an intense laser pulse. This however leads to the production of debris which can cause major degradation of expensive EUV / SXR mirrors. Different techniques to minimize debris have been proposed [2] such as mixed composition targets [17, 18] and liquid tin mirrors as collectors [19]. Indeed it may be possible to extend these approaches into the SXR region, e.g. the liquid tin mirror being developed for 13.5 nm could be a prototype for elements at other wavelengths.

The recording of the 4d - 4f emission in cesium through lutetium showed that these relatively narrow regions of resonance-like emission became more complex and moved to shorter wavelength with increasing nuclear charge Z [20, 21]. In order to interpret such complicated spectra, Mandelbaum *et al* [22] employed the unresolved transition array (UTA) approach developed by Bauche-Arnoult, Bauche and Klapisch [23–26] and concluded that interactions between the $4p^6\ 4d^{N-1}\ 4f$ and $4p^5\ 4d^{N+1}$ configurations are responsible for narrowing the transition arrays and their superposition in adjacent ion stages. In this work we adopt the UTA approach to characterize the emission arising from 4d - 4f and 4p - 4d transitions in Pd-like to Rb-like ions of hafnium through actinium ($Z = 72 - 89$). Of these elements tungsten and gold have received most attention to date owing to their use in the fusion community [27–31]. Tungsten is currently being

used in the walls of the divertor in many magnetic confinement fusion devices, such as tokamaks, to reduce tile erosion [29, 32, 33]. However even small quantities of tungsten contaminating the core plasma ($> 10^{-5}$ [34]) can seriously limit the energy confinement in a fusion reactor. Knowledge of the W emission radiated from each ion stage in the plasma core is therefore essential to eradicate this degradation. Gold is used for indirectly driven inertial confinement fusion (ICF), where laser radiation heats the inside of a Au hohlraum producing a plasma which emits intense x-rays. Therefore knowledge of Au radiative opacity is crucial to the success of ICF [30, 31].

Recent experiments have employed the LPP technique using metal targets to generate EUV/SXR radiation. For example a bulk rhenium target was used to develop new SXR microscopy applications in the "carbon window"($\lambda \approx 4.5 - 5$ nm) [35]. Also a solid gold-based LPP source was utilized in the design of an EUV source and optics setup to achieve high energy density and spatial resolution in a compact setup [36]. In [37] the emitted X-ray spectra of different target materials were recorded over the wavelength range of $0.8-18$ nm. Low-Z elements (Cu, Ti, Fe, and Al) resulted in intense line emission, while continuum-like emission was detected from higher-Z materials (Mo and Ag). Therefore it is possible to optimize the brilliance of the LPP source for a specific x-ray emission range and a particular application of interest.

The outline of this paper is as follows: In section 2, 180 theoretical 4d - 4f and 4p - 4d unresolved transition array (UTA) spectra are presented, for ions with configurations $4p^6\ 4d^N$ - $4p^6\ 4d^{N-1}\ 4f$ and $4p^6\ 4d^N$ - $4p^5\ 4d^{N+1}$, $N = 1..10$. The effects of configuration interaction (CI), and overall trends in the position and intensity of UTA peaks from hafnium to actinium are discussed. In section 3 UTA statistics, namely, mean wavelength $\bar{\lambda}_{gA}$ and spectral width $\Delta\lambda_{gA}$ for the above ions are calculated which allows us to characterize these possible EUV / SXR sources. The gradual separation of the 4d - 4f UTA from the 4p - 4d UTA is highlighted. Finally in section 4 we conclude with a summary of this work.

2. Unresolved Transition Arrays of Ions with $Z = 72 - 89$

As noted in [14] the strongest lines occurring in the EUV result from 4d - 4f and 4p - 4d transitions in ion stages with open 4d subshells. Calculations were performed with the flexible atomic code (FAC) [38, 39], a complete software package developed for the computation of various atomic collisional and radiative processes to model spectral emission from astrophysical plasmas. Since its introduction however it has been successfully applied in numerous additional fields e.g. magnetic fusion and laser produced plasmas. FAC combines the strengths of existing atomic codes e.g. ATOM [40], HULLAC [41] and SZ [42, 43]; it uses a fully relativistic approach based on the Dirac equation, and implements efficient methods for distorted wave approximation, thus allowing its application to ions with large values of nuclear charge. The following basis set was used: $4p^6\ 4d^N$, $4p^6\ 4d^{N-1}$ nl and $4p^5\ 4d^{N+1}$ where $n \leq 8$, $l \leq 3$ and $1 \leq N \leq 10$. Figures 1 - 3 show Pd-like through Rb-like spectra of hafnium through

actinium including CI. 4d - 4f transitions are shown in black, 4p - 4d transitions are shown in orange (gray) and all other transitions are shown in yellow (light gray). It was noted in [14] that for a given element, the emission from 4d - 4f and 4p - 4d becomes stronger and more concentrated within a particular wavelength range when configuration interaction is included. It is well known that CI redistributes transitions providing a more accurate description of experimental spectra [44]. However as Z increases there was little discernable difference between the spectra excluding CI and including CI. This point will be further developed under the UTA framework in section 3. Figure 4 displays the maximum peak emission (in terms of gA values) for (a) 4d - 4f transitions and (b) 4p - 4d transitions for each element as a function of wavelength. As was observed for the lanthanides [14, 20–22], both 4d - 4f and 4p - 4d emission moves to shorter wavelength on increasing Z. The dependence of peak transition energies on atomic number Z is presented in Figure 4 (c). This shows that on increasing Z, the 4d - 4f emission peak and the 4p - 4d emission peak clearly separate. However, the fact that the maximum gA value remains relatively comparable for each transition type over the range of $Z = 72 - 89$, implies that these elements could be potential radiation sources over the wavelength range $\lambda = 2.5 - 6$ nm. This point is further quantified with the aid of UTA statistical analysis in the following section.

3. Unresolved Transition Array Statistics of Ions with $Z = 72 - 89$

In order to quantify the emission from the 4d - 4f and 4p - 4d transitions in these ions, we adopted the unresolved transition array (UTA) approach developed by Bauche-Arnoult, Bauche and Klapisch [23–26]. UTAs were introduced originally to aid interpretation of low resolution soft X-ray spectra emitted by hot plasmas. They are currently widely used to approximate complex atomic spectra in plasma opacity and emissivity calculations which reduces computation times in large-scale radiation hydrodynamic simulations of plasma dynamics. In the UTA model, the discrete line spectra are replaced by a continuous function (usually Gaussian) such that each configuration-configuration transition array is characterized by the average quantities such as total intensity, average transition energy and variance. The average and variance of the transition energies ($\bar{E}$ and σ^2 respectively) can be expressed as the gA-weighted sums

$$\bar{E} = \frac{\sum\limits_{j,i<j} g_j A_{ji} E_{ij}}{\sum\limits_{j,i<j} g_j A_{ji}} \tag{1}$$

and

$$\sigma^2 = \frac{\sum\limits_{j,i<j} g_j A_{ji} (\bar{E} - E_{ij})^2}{\sum\limits_{j,i<j} g_j A_{ji}}, \tag{2}$$

where A_{ji} is the Einstein coefficient for spontaneous emission from level j to level i, and g_j is the statistical weight of the upper level. The mean wavelength $\bar{\lambda}_{gA}$ and the

spectral width $\Delta\lambda_{gA}$ of the transition array can be defined as follows

$$\bar{\lambda}_{gA} = 10^8/\bar{E}, \tag{3}$$

$$\Delta\lambda_{gA} = \sqrt{8ln2} \times 10^8\sigma/\bar{E}^2, \tag{4}$$

where $\bar{E}$ and σ are expressed in cm^{-1} and $\bar{\lambda}_{gA}$ and $\Delta\lambda_{gA}$ in $\mathring{A}$.

Before applying the above UTA analysis, it is worthwhile to demonstrate the accuracy of the FAC code and the validity of its use in the current work. As an example, the $4p^6$ 4d - $4p^5$ $4d^2$ and $4p^6$ 4d - $4p^6$ 4f transition wavelengths and UTA statistics of the Rb-like tungsten ion, W^{37+} are presented in Table 1. This is a suitable choice owing to recent interest in it by members of the fusion community. As such wavelengths from a number of sources are available and it can be seen that the results of the current theoretical work compare favorably with experimentally recorded values. The $4p^6$ 4d - $4p^5$ $4d^2$ and $4p^6$ 4d - $4p^6$ 4f transitions were first identified by Radtke *et al* [29] using an electron-beam ion trap at a wavelength uncertainty of $\pm 0.05\mathring{A}$. Later Utter *et al* [45] improved on this by recording at a higher spectral resolution with wavelength uncertainties of between ± 0.004 and $\pm 0.02\mathring{A}$. In the work of Radtke *et al* [29], *ab initio* theoretical calculations were carried out using the multiconfigurational relativistic HULLAC code [46, 47] and the difference between measured and calculated wavelengths was found to be as much as $1\mathring{A}$. The current calculations employ the FAC code which has an accuracy of 10 - 30 m$\mathring{A}$ at $10\mathring{A}$ [48]. The wavelengths calculated with the FAC code are in closer agreement with experimental values, where the largest difference is found to be $0.6\mathring{A}$. Also presented in Table 1 is the UTA analysis for W^{37+} where (i) denotes the results of Radtke *et al* [29] obtained using the HULLAC code, and (ii) refers to results obtained by application of 1- 4 to the FAC data produced in the current work. Agreement is good with a maximum difference of $0.16\mathring{A}$ in the spectral width of the mixed CI transition array ($4p^6$ 4d - [$4p^5$ $4d^2$ + $4p^6$ 4f]). This can be attributed to the use of a larger basis set in the current work, as described in Section 2. As was the approach in [12], this basis set was chosen for consistency when surveying such a large number of ions. Inclusion of various configurations will continue as and when more detailed experimental energy levels, transition wavelengths and line strengths of these ions become available for comparison.

The above discussion indicates that the use of the FAC code is appropriate for producing the 180 theoretical ionic spectra considered here. It also shows that these spectra can be adequately described using the UTA approach. The 4d - 4f and 4p - 4d UTAs were extracted from the CI spectra and the above statistical analysis was applied to each separately. The results are displayed in Figure 5, excluding CI (left) and including CI (right), and Tables 2 and 3. Figure 5 shows the dependence of mean wavelength ($\bar{\lambda}_{gA}$) on ion stage for each element with $Z = 72 - 89$ (4d - 4f in black and 4p - 4d in red). A number of observations can be made from these results: (i) CI effects are more dramatic in lower Z elements, (ii) CI concentrates the 4p - 4d UTA at a particular wavelength for this series of ions, for example, in hafnium which is plotted

in Figure 5 (c) non-CI and (d) CI. For the 4p - 4d UTA, $\bar{\lambda}_{gA}$ varies from 5.29 - 5.86 nm in the non-CI case compared to 5.17 - 4.82 nm in the CI case. For the 4d - 4f UTA, $\bar{\lambda}_{gA}$ varies from 6.43 - 5.09 nm in the non-CI case compared to 6.26 - 5.06 nm in the CI case. (iii) CI effects the 4p - 4d UTA positioning more than the 4d - 4f in hafnium. This can be observed for many of the lower Z elements in this study. Gradually the effects of CI are diminished as can be seen by comparing Figure 5 (a) and (b). Finally by actinium we see very little variation between CI and non-CI results. For the 4p - 4d UTA, $\bar{\lambda}_{gA}$ varies from 2.79 - 2.98 nm in the non-CI case compared to 2.77 - 2.54 nm in the CI case. For the 4d - 4f UTA, $\bar{\lambda}_{gA}$ varies from 4.27 - 3.40 nm in the non-CI case compared to 3.88 - 3.39 nm in the CI case. These results are summarized for the CI case only in Tables 2 and 3. The mean wavelength $\bar{\lambda}_{gA}$ and spectral width $\Delta\lambda_{gA}$ for 4d - 4f and 4p - 4d UTAs calculated from the CI spectra are presented. From these values and the results presented in Figure 4, it is possible to identify strong emitters for almost all wavelengths between approximately $\lambda = 2.5 - 6$ nm. Indeed in some cases it is possible that a target of mixed composition may give broad band emission across this wavelength range encompassing the "water window" and soft X-ray region.

4. Conclusion

Possible extreme ultraviolet and soft X-ray radiation sources were identified, using the FAC relativistic code, as emission peaks arising from 4d - 4f and 4p - 4d transitions in Pd-like to Rb-like ions of hafnium through actinium. For increasing nuclear charge, these strong emitters are seen to separate and move to shorter wavelength. The emission was comparable from each source and was characterized using the unresolved transition array model. The laser produced plasma technique may be employed in future work to generate these radiation sources which find application in numerous exciting fields, e.g. microscopy, spectroscopy and lithography.

Acknowledgments

This work was supported by Science Foundation Ireland under Principal Investigator research grant 07/IN.1/B1771. The author thanks G. O'Sullivan for helpful discussions.

5. References

[1] Churilov S S, Joshi Y N, Reader J and Kildiyarova R R 2004 $4p^64d^8$-($4d^75p$+$4d^74f$+$4p^54d^9$) transitions in Xe XI *Phys. Scr.* **70** 126

[2] Bakshi V ed 2006 *EUV sources for lithography* SPIE Press Monograph vol PM149 (Bellingham WA: SPIE Press)

[3] O'Sullivan G, Cummings A, Dong C Z, Dunne P, Hayden P, Morris O, Sokell E, O'Reilly F, Su M G and White J 2009 Emission and absorption in laser produced plasmas: processes and applications *J. Phys.: Conf. Ser.* **163** 012003

[4] Sasaki A, Sunahara A, Furukawa H, Nishihara K, Fujioka S, Nishikawa T, Koike F, Ohasni H and Tanuma H 2010 Modeling of radiative properties of Sn plasmas for extreme-ultraviolet source *J. Appl. Phys.* **107** 113303

[5] Böwering N, Martins M, Partlo W N and Fomenkov I V 2004 Extreme ultraviolet emission spectra of highly ionized xenon and their comparison with model calculations *J. Appl. Phys.* **95** 16

[6] Churilov S S and Ryabtsev A N 2006 *Analyses of the Sn IX - Sn XII spectra in the EUV region Phys. Scr.* **73** 614

[7] Poirier M, Blenski T, de Gaufridy de Dortan F and Gilleron F 2006 Modeling of EUV emission from xenon and tin plasma sources for nanolithography *J. Quant. Spectrosc. Radiat. Transfer* **99** 482

[8] F. de Gaufridy de Dortan 2007 Influence of configuration interaction on satellite lines of xenon and tin in the EUV region *J. Phys. B: At. Mol. Opt. Phys.* **40** 599

[9] Churilov S S, Kilidiyarova R R, Ryabtsev A N and Sadovsky S V 2009 EUV spectra of Gd and Tb ions excited in laser-produced and vacuum spark plasmas *Phys. Scr.* **80** 045303

[10] Otsuka T, Kilbane D, White J, Higashiguchi T, Yugami N, Yatagai T, Jiang W, Endo A, Dunne P and O'Sullivan G 2010 Rare-earth plasma extreme ultraviolet sources at 6.5 - 6.7 nm *Appl. Phys. Lett.* **97** 111503

[11] Otsuka T, Kilbane D, Higashiguchi T, Yugami N, Yatagai T, Jiang W, Endo A, Dunne P and O'Sullivan G 2010 Systematic investigation of self-absorption and conversion efficiency of 6.7 nm extreme ultraviolet sources *Appl. Phys. Lett.* **97** 231503

[12] Kilbane D and O'Sullivan G 2010 Extreme ultraviolet emission spectra of Gd and Tb ions *J. Appl. Phys.* **108** 104905

[13] Sasaki A, Nishihara K, Sunahara A, Furukawa H, Nishikawa T and Koike F 2010 Theoretical investigation of the spectrum and conversion efficiency of short wavelength extreme-ultraviolet light sources based on terbium plasmas *Appl. Phys. Lett.* **97** 231501

[14] D. Kilbane and G. O'Sullivan 2010 Ground-state configurations and unresolved transition arrays in extreme ultraviolet spectra of lanthanide ions *Phys. Rev.* A **82** 062504

[15] Wachulak P W, Bartnik A, Fiedorowicz H, Rudawski P, Jarocki R, Kostecki K, and Szczurek M 2010 'Water window' compact, table-top laser plasma soft X-ray sources based on a gas puff target *Nucl. Instrum. Methods Phys. Res. B* **268** 1692

[16] Da Silva L B, Trebes J E, Balhorn R, Mrowka S, Anderson E, Attwood D T, Barbee Jr. T W, Brase J, Corzett M, Gray J,Koch J A, Lee C, Kern D, London R A, MacGowan B J and Mathews D L 1992 X-ray laser microscopy of rat sperm nuclei *Science* **258** 269

[17] Hayden P, Cummings A, Murphy N, O'Sullivan G, Sheridan P, White J and Dunne P 2006 13.5 nm extreme ultraviolet emission from tin based laser produced plasma sources *J. Appl. Phys.* **99** 093302

[18] Rakowski R, Bartnik A, Fiedorowicz H, de Gaufridy de Dortan F, Jarocki R, Kostecki J, Mikołajczyk J, Ryé L, Szcurek M and Wachulak P 2010 Characterization and optimization of the laser-produced plasma EUV source at 13.5 nm based on a double-stream Xe/He gas puff target *Appl. Phys. B: Lasers and Optics* **101** 773

[19] Fahy K, O'Reilly F, Scally E and Sheridan P 2010 Robust liquid metal collector mirror for EUV and soft x-ray plasma sources *SPIE* **7802** 78020K

[20] O'Sullivan G and Carroll P K 1981 4d-4f emission resonances in laser-produced plasmas *J. Opt. Soc. Am.* **71** 227

[21] Carroll P K and O'Sullivan G 1982 Ground-state configurations of ionic species I through XVI for Z=57-74 and the interpretation of 4d-4f emission resonances in laser-produced plasmas *Phys. Rev.* A **25** 275

[22] Mandelbaum P, Finkenthal M, Schwob J L and Klapisch M 1987 Interpretation of the quasicontinuum band emitted by highly ionized rare-earth elements in the 70 - 100 - *Å* range *Phys. Rev.* A **35** 5051

[23] Bauche-Arnoult C, Bauche J and Klapisch M 1979 Variance of the distributions of energy levels

and of the transition arrays in atomic spectra *Phys. Rev.* A **20** 2424

[24] Bauche-Arnoult C, Bauche J and Klapisch M 1982 Variance of the distributions of energy levels and of the transition arrays in atomic spectra. II. Configurations with more than two open subshells *Phys. Rev.* A **25** 2641

[25] Bauche J, Bauche-Arnoult C, Luc-Koenig E, Wyart J-F and Klapisch M 1983 Emissive zones of complex atomic configurations in highly ionized atoms *Phys. Rev.* A **28** 829

[26] Bauche-Arnoult C, Bauche J and Klapisch M 1985 Variance of the distributions of energy levels and of the transition arrays in atomic spectra. III. Case of spin-orbit-split arrays *Phys. Rev.* A **31** 2248

[27] Mandelbaum P, Schwob J L, Finkenthal M and Klapisch M 1988 Analysis of quasi-continuum bands and line spectra of highly ionized W and Au *J. Phys. Colloq.* **49** C1 217

[28] Biedermann C, Radtke R, Schwob J-L, Mandelbaum P, Doron R, Fuchs T and Fußmann G 2001 EUV spectroscopy of highly charged tungsten ions relevant to hot plasmas *Phys. Scr.* **T92** 85

[29] Radtke R, Biedermann C, Schwob J L, Mandelbaum P and Doron R 2001 Line and band emission from tungsten ions with charge 21+ to 45+ in the 45 - 70 - $\AA$ range *Phys. Rev.* A **64** 012720

[30] Zeng J and Yuan J 2006 Radiative opacity of gold plasmas studied by a detailed level-accounting method *Phys. Rev.* E **74** 025401(R)

[31] Zeng J and Yuan J 2007 Spectrally resolved opacities and Rosseland and Planck mean opacities of lowly ionized gold plasmas: A detailed level-accounting investigation *Phys. Rev.* E **76** 026401

[32] Field A R, Fussmann G, Garcia-Rosales C, Hirsch S, Lieder G, Naujoks D, Neu R, Pitcher C S, Radtke R, Wenzel U and the ASDEX-Upgrade Team 1995 Studies of divertor target plate erosion in the ASDEX-Upgrade tokamak *J. Nucl. Mater.* **220** 553

[33] Naujoks D, Asmussen K, Bessenrodt-Weberpals M, Deschka S, Dux R, Engelhardt W, Field A R, Fussmann G, Fuchs J C, Garcia-Rosales C, Hirsch S, Ignacz P, Lieder G, Mast K F, Neu R, Radtke R, Roth J, Wenzel U and the ASDEX-Upgrade Team 1996 Tungsten as target material in fusion devices *Nucl. Fusion* **36** 671

[34] Peacock N J, Barnsley R, Hawkes N C, Lawson K D and O'Mullane M G 1996 *Diagnostics for Experimental Thermonuclear Fusion Reactors* 291 ed Scott P E, Giuseppe G and Sindoni E (Plenum Press, New York)

[35] Artyukov I A, Feschenko R M, Vinogradov A V, Bugayev Ye A, Devizenko O Y, Kondratenko V V, Kasyanov Yu S, Hatano T, Yamamoto M and Saveliev S V 2010 Soft X-ray imaging of thick carbon-based materials using the normal incidence multilayer optics *Micron* **41** 722

[36] Bayer A, Barkusky F, Döring S, Großmann P and Mann K 2010 Applications of compact laser-driven EUV/XUV plasma sources *X-Ray Opt. Instrum.* **2010** 687496

[37] Mantouvalou I, Jung R, Tuemmler J, Legall H, Bidu T, Stiel H, Malzer W, Kanngießer B and Sandner W 2011 Note: Study of extreme ultraviolet and soft x-ray emission of metal targets produced by laser-plasma-interaction *Rev. Sci. Instrum.* **82** 066103

[38] Gu M F 2003 Indirect X-ray line-formation processes in iron L-shell ions *Astrophys. J.* **582** 1241

[39] Gu M F 2008 The flexible atomic code *Can. J. Phys.* **86** 675

[40] Amusia M Y and Chernysheva L V 1997 *Computation of atomic processes: A handbook for ATOM programs.* (Institute of Physics Publishing, Bristol, UK)

[41] Bar-Shalom A, Kalpisch M and Oreg J 2001 HULLAC, an integrated computer package for atomic processes in plasmas *J. Quant. Spectrosc. Radiat. Transfer* **71** 169

[42] Sampson D H, Zhang H L, Mohanty A K and Clark R E H 1989 A Dirac-Fock-Slater approach to atomic structure for highly charged ions *Phys. Rev.* A **40** 604

[43] Zhang H L, Sampson D H and Mohanty A K 1989 Fully relativistic and quasirelativistic distorted-wave methods for calculating collision strengths for highly charged ions *Phys. Rev.* A **40** 616

[44] Cowan R D 1981 *The Theory of Atomic Structure and Spectra* (University of California Press, Berkeley, CA)

[45] Utter S B, Beiersdorfer P and Träbert E 2002 Electron-beam ion-trap spectra of tungsten in the EUV *Can. J. Phys.* **80** 1503

[46] Bar-Shalom A, Klapisch M and Goldstein W H 1988 *The HULLAC code for atomic physics* (unpublished)
[47] Bar-Shalom A, Klapisch M and Oreg J 1988 Electron collision excitations in complex spectra of ionized heavy atoms *Phys. Rev.* A **38** 1773
[48] Gu M F 2003 *FAC 1.1.0 manual*
[49] Kramida A E and Shirai T 2009 Energy levels and spectral lines of tungsten, W III through W LXXIV *At. Data and Nucl. Data Tables* **95** 305

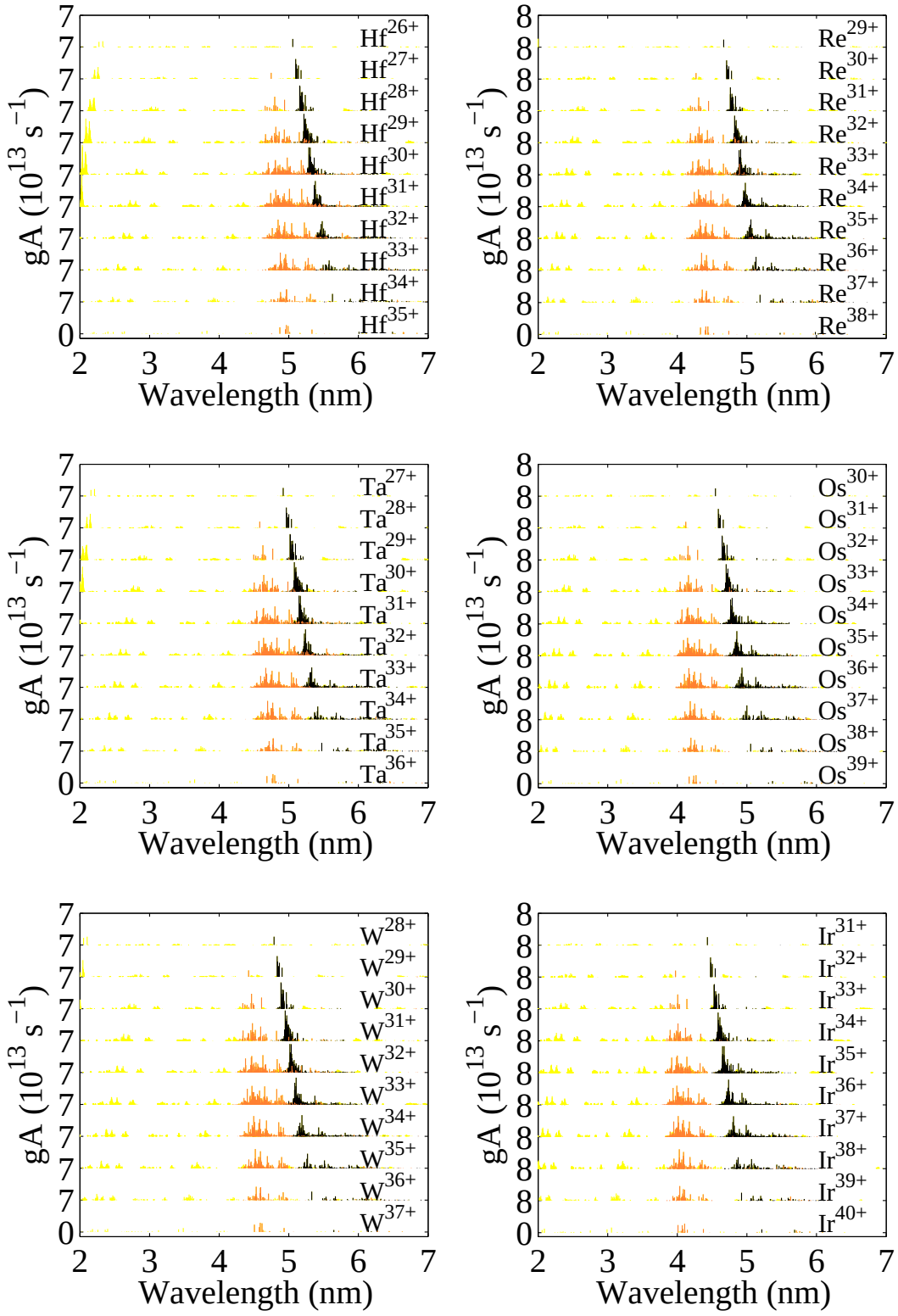

Figure 1. (Color online) Pd-like through Rb-like spectra of hafnium through iridium computed with the FAC code including CI. Black denotes 4d - 4f transitions, orange (gray) denotes 4p - 4d transitions and yellow (light gray) denotes all transitions.

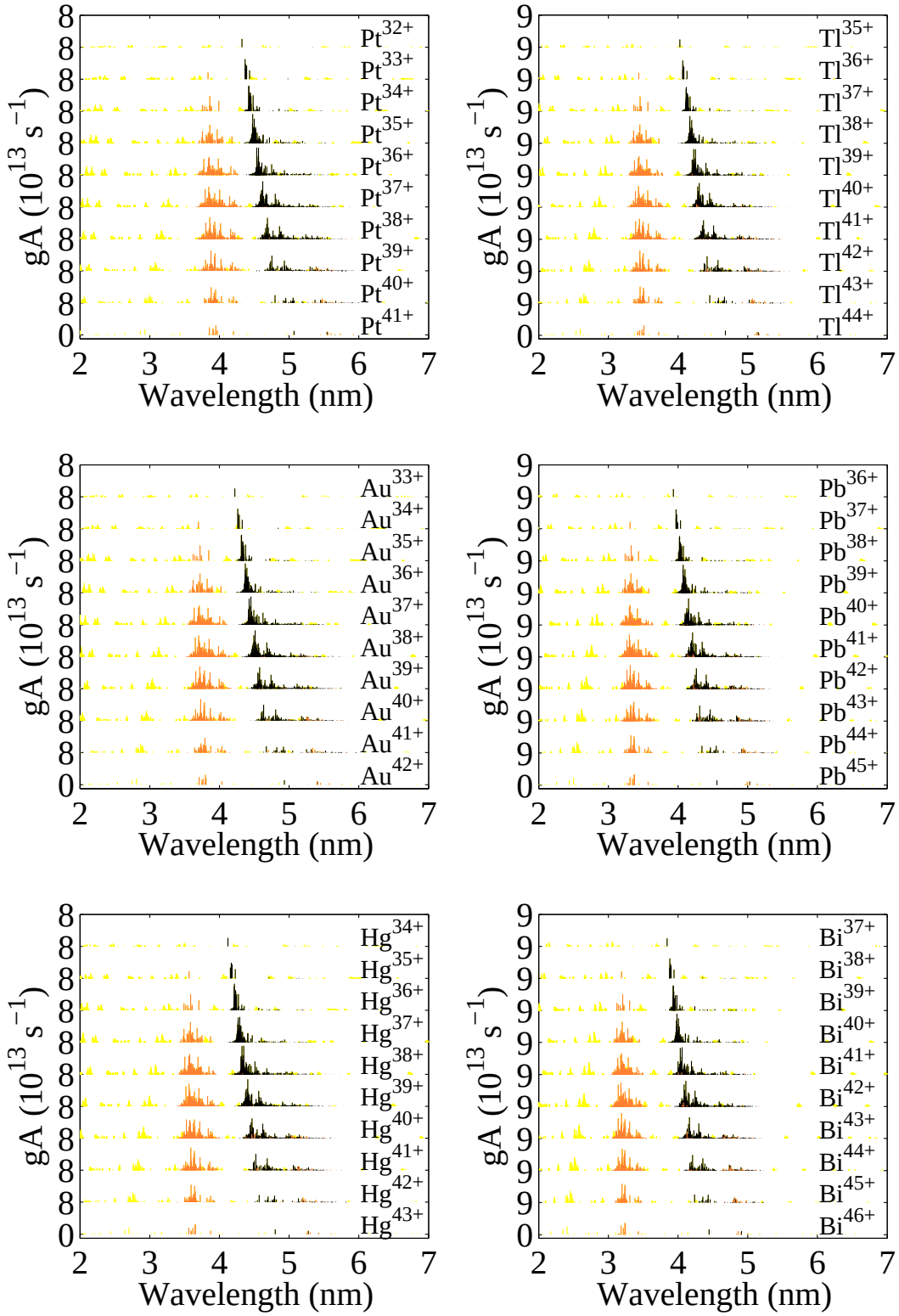

Figure 2. (Color online) Pd-like through Rb-like spectra of platinum through bismuth computed with the FAC code including CI. Black denotes 4d - 4f transitions, orange (gray) denotes 4p - 4d transitions and yellow (light gray) denotes all transitions.

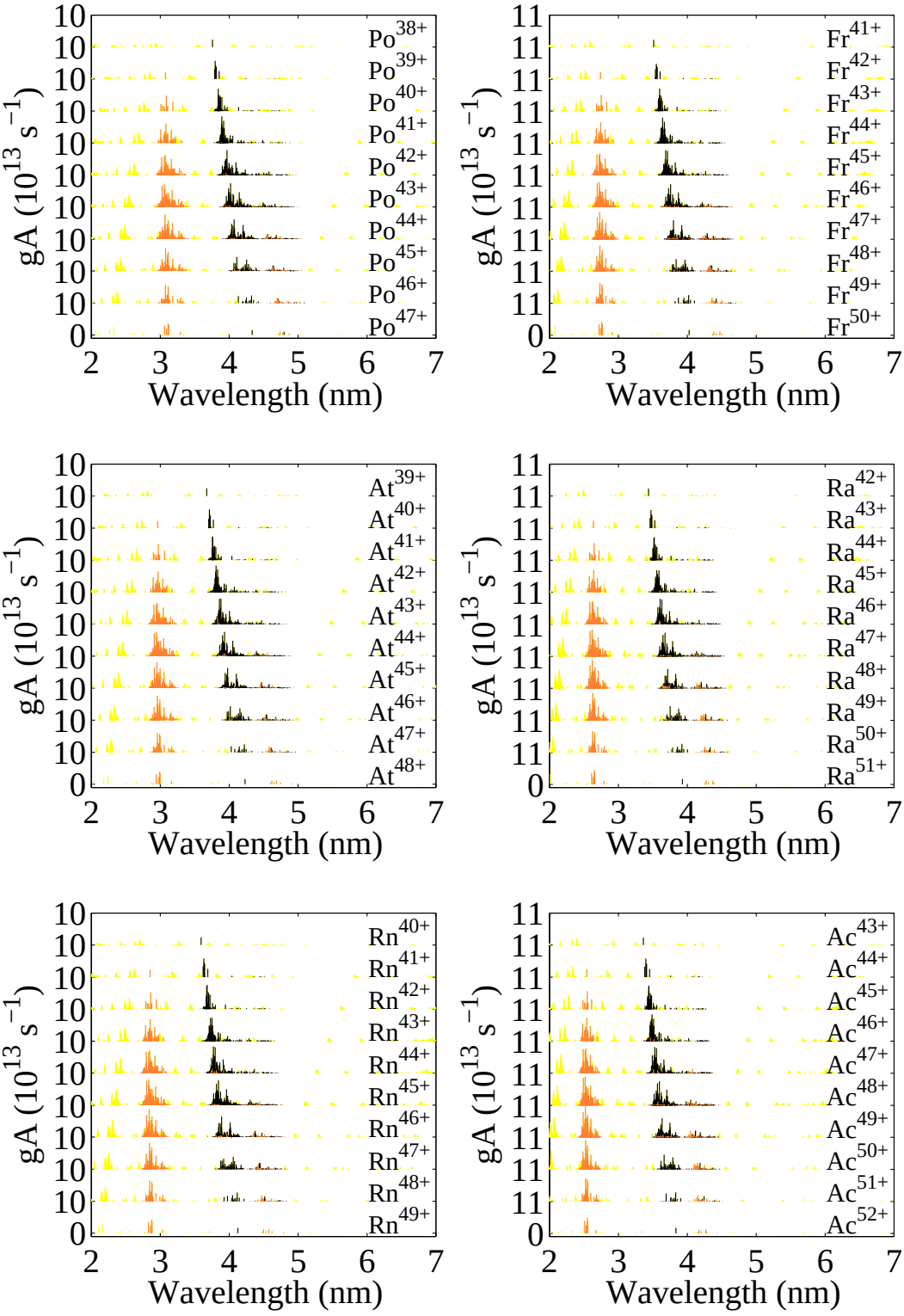

Figure 3. (Color online) Pd-like through Rb-like spectra of polonium through actinium computed with the FAC code including CI. Black denotes 4d - 4f transitions, orange (gray) denotes 4p - 4d transitions and yellow (light gray) denotes all transitions.

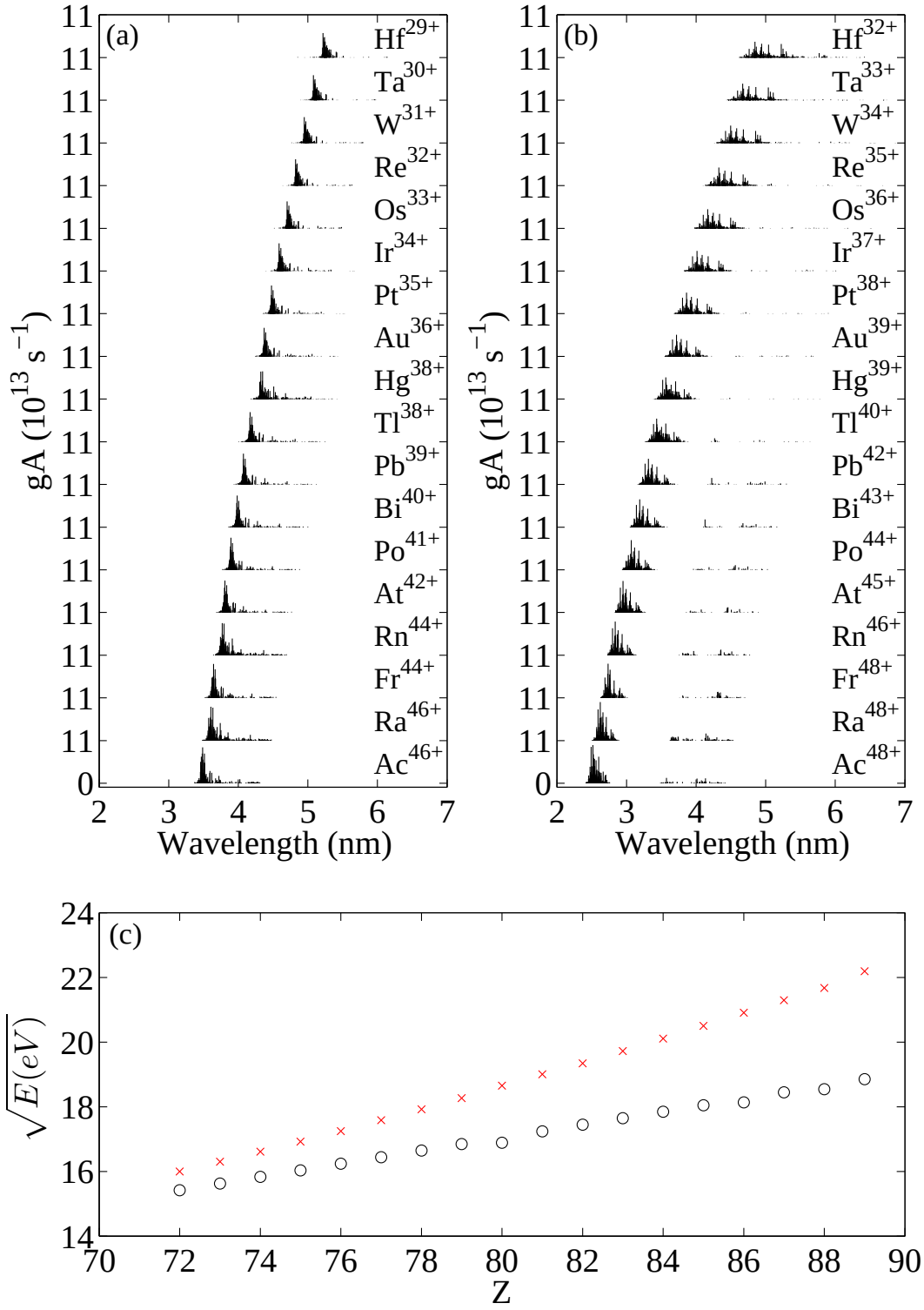

Figure 4. (Color online) Maximum peak emission from (a) 4d - 4f and (b) 4p - 4d UTAs (including CI) in elements with $Z = 72-89$. (c) Dependence of UTA transition energies on atomic number Z, 4d - 4f (black open circles), 4p - 4d (red crosses).

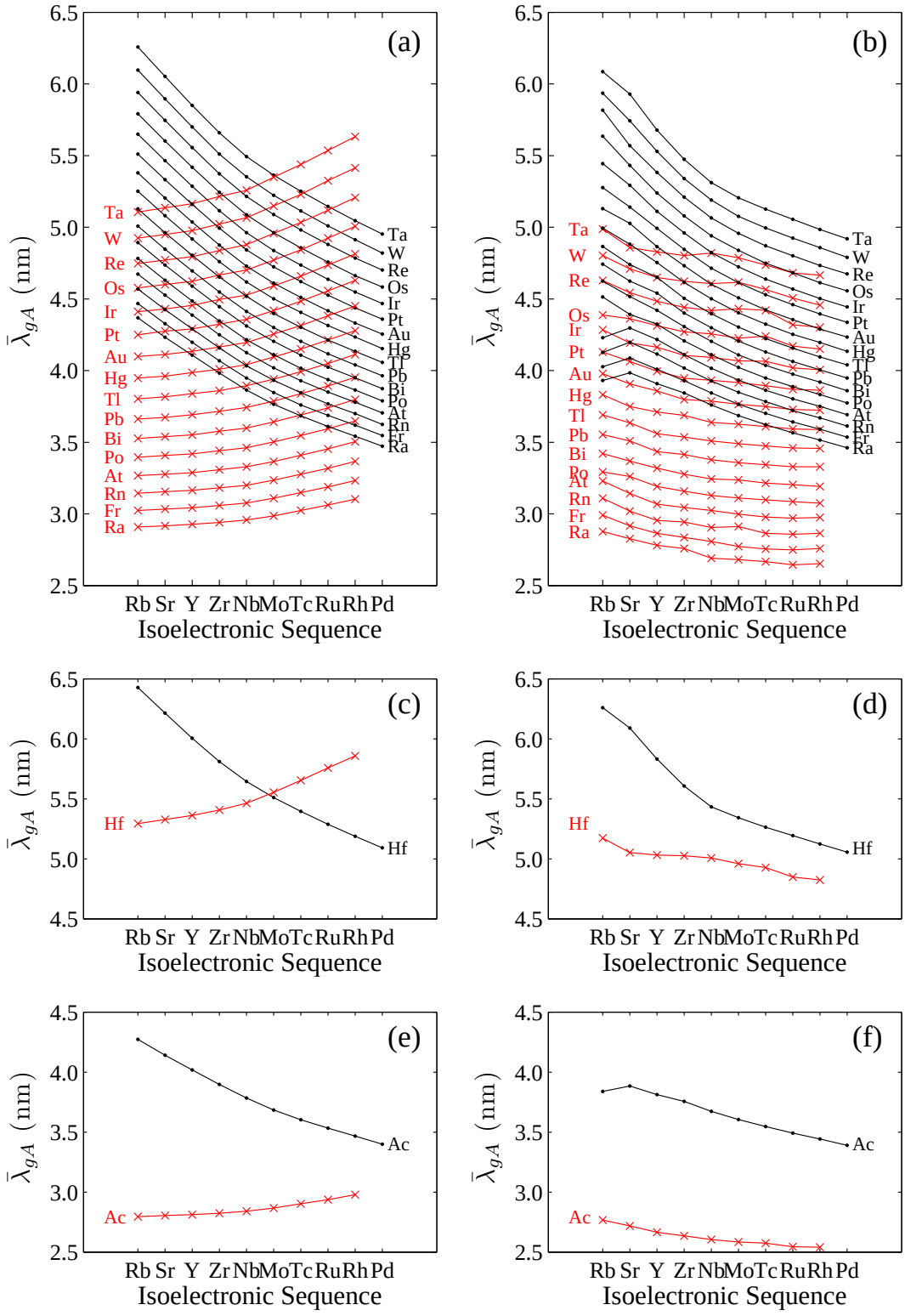

Figure 5. (Color online) Dependence of mean wavelength ($\bar{\lambda}_{gA}$) on ion stage for elements with $Z = 72 - 89$ (4d - 4f UTA black dot, 4p - 4d UTA red cross): (a) tantalum through radium non-CI, (b) tantalum through radium CI, (c) hafnium non-CI, (d) hafnium CI, (e) actinium non-CI and (f) actinium CI.

Table 1. Transition wavelengths and UTA statistics of Rb-like tungsten, W^{37+}. (a) Transition wavelengths: In column (i) λ_{exp} and λ_{th} respectively, denote the experimental and theoretical transition wavelengths obtained by Radtke *et al* [29]. The theoretical values were calculated using the HULLAC code. In column (ii) λ_{th} denotes theoretical wavelengths calculated in the present work using the FAC code. In column (iii) λ_{exp} refers to transition wavelengths recorded experimentally by Utter *et al* [45] and presented by Kramida and Shirai in [49]. (b) UTA statistics: Calculated mean wavelength $\bar{\lambda}_{gA}$ and spectral width $\Delta\lambda_{gA}$ for the unresolved transition arrays. Column (i) denotes values from Radtke *et al* [29] and column (ii) denotes values obtained by applying 1- 4 to the FAC data produced in the current work. Wavelengths throughout the table are given in $\mathring{A}$.

(a)	(i)		(ii)	(iii)
Transition	λ_{exp}	λ_{th}	λ_{th}	λ_{exp}
$4p^6\ 4d\ {}^2D_{3/2}$ - $4p^5({}^2P^o_{1/2})\ 4d^2({}^3F_2)\ (1/2,2)^o_{5/2}$	49.52	49.06	49.32	49.641
$4p^6\ 4d\ {}^2D_{3/2}$ - $4p^6\ 4f\ (0,5/2)\ ^o_{5/2}$	56.86	56.04	56.46	56.880
$4p^6\ 4d\ {}^2D_{3/2}$ - $4p^5({}^2P^o_{3/2})\ 4d^2({}^3F_4)\ (3/2,4)^o_{5/2}$	57.74	56.72	57.16	57.755
$4p^6\ 4d\ {}^2D_{3/2}$ - $4p^5({}^2P^o_{3/2})\ 4d^2({}^3F_3)\ (3/2,3)^o_{3/2}$	64.82	63.87	64.40	64.825

(b)	(i)		(ii)	
Unresolved transition array	$\bar{\lambda}_{gA}$	$\Delta\lambda_{gA}$	$\bar{\lambda}_{gA}$	$\Delta\lambda_{gA}$
$4p^6\ 4d$ - $4p^5\ 4d^2$	49.18	14.28	49.23	14.22
$4p^6\ 4d$ - $4p^6\ 4f$	60.93	5.15	60.96	5.18
Mixed	49.00	13.16	49.01	13.00

Table 2. Calculated mean wavelength $\bar{\lambda}_{gA}$ and spectral width $\Delta\lambda_{gA}$ for the configuration interaction unresolved transition arrays of hafnium through mercury ions: Rb-like to Rh-like ions for the 4p - 4d arrays and Rb-like to Pd-like ions for the 4d - 4f arrays. Wavelengths throughout the table are given in $\mathring{A}$.

4p - 4d	Hf		Ta		W		Re		Os		Ir		Pt		Au		Hg	
Ion	$\bar{\lambda}_{gA}$	$\Delta\lambda_{gA}$	$\bar{\lambda}_{gA}$	$\Delta\lambda_{gA}$	$\bar{\lambda}_{gA}$	$\Delta\lambda_{gA}$	$\bar{\lambda}_{gA}$	$\Delta\lambda_{gA}$	$\bar{\lambda}_{gA}$	$\Delta\lambda_{gA}$	$\bar{\lambda}_{gA}$	$\Delta\lambda_{gA}$	$\bar{\lambda}_{gA}$	$\Delta\lambda_{gA}$	$\bar{\lambda}_{gA}$	$\Delta\lambda_{gA}$	$\bar{\lambda}_{gA}$	$\Delta\lambda_{gA}$
Rb-like	51.72	11.13	49.87	11.21	48.03	11.12	46.29	11.06	43.86	9.21	42.85	10.94	41.29	11.02	39.78	11.03	38.31	10.98
Sr-like	50.52	6.94	48.57	6.73	47.10	8.08	45.44	8.48	43.62	8.08	41.92	7.91	40.63	8.83	39.07	8.62	37.49	8.40
Y-like	50.31	6.22	48.27	5.68	46.49	5.89	44.83	6.33	43.13	6.33	41.63	6.80	39.95	6.33	38.57	6.84	37.11	6.72
Zr-like	50.26	6.01	48.02	4.79	46.22	4.85	44.41	4.42	42.70	4.35	41.06	4.21	39.46	3.79	37.98	3.94	36.88	5.65
Nb-like	50.06	5.87	48.20	5.76	46.07	4.73	44.19	4.06	42.56	4.21	40.92	3.93	39.32	3.43	37.87	3.65	36.38	3.13
Mo-like	49.59	5.58	47.86	5.62	46.16	5.58	44.31	5.03	42.27	3.45	40.68	3.22	39.16	3.19	37.65	2.67	36.25	2.84
Tc-like	49.28	5.70	47.37	5.28	45.66	5.23	44.20	5.43	42.41	4.97	40.65	4.15	38.94	2.78	37.49	2.70	36.09	2.53
Ru-like	48.47	5.17	46.81	5.24	45.06	4.85	43.19	3.02	41.70	3.52	40.19	3.34	38.70	2.66	37.29	2.51	35.92	2.35
Rh-like	48.24	7.28	46.65	7.36	44.56	5.26	43.01	5.11	41.51	4.95	40.04	4.77	38.62	4.57	37.23	4.35	35.88	4.09

4d - 4f	Hf		Ta		W		Re		Os		Ir		Pt		Au		Hg	
Ion	$\bar{\lambda}_{gA}$	$\Delta\lambda_{gA}$	$\bar{\lambda}_{gA}$	$\Delta\lambda_{gA}$	$\bar{\lambda}_{gA}$	$\Delta\lambda_{gA}$	$\bar{\lambda}_{gA}$	$\Delta\lambda_{gA}$	$\bar{\lambda}_{gA}$	$\Delta\lambda_{gA}$	$\bar{\lambda}_{gA}$	$\Delta\lambda_{gA}$	$\bar{\lambda}_{gA}$	$\Delta\lambda_{gA}$	$\bar{\lambda}_{gA}$	$\Delta\lambda_{gA}$	$\bar{\lambda}_{gA}$	$\Delta\lambda_{gA}$
Rb-like	62.60	5.70	60.85	5.84	59.35	5.95	58.17	5.90	56.35	6.05	54.44	5.77	52.77	5.65	51.29	5.56	49.93	5.49
Sr-like	60.90	8.55	59.28	8.24	57.42	8.00	55.69	7.51	54.32	7.35	52.93	7.09	51.40	6.85	50.26	6.64	48.82	6.29
Y-like	58.31	7.92	56.77	7.54	55.30	7.18	53.83	6.59	52.38	6.35	51.11	6.40	49.92	6.32	48.65	6.12	47.53	5.98
Zr-like	56.06	6.22	54.74	5.99	53.39	5.72	52.10	5.67	50.79	5.45	49.61	5.39	48.44	5.36	47.31	5.34	46.14	5.16
Nb-like	54.34	4.01	53.11	4.15	51.89	4.25	50.65	4.22	49.39	4.08	48.23	4.11	47.14	4.26	46.02	4.20	45.00	4.34
Mo-like	53.42	2.66	52.06	2.80	50.76	2.85	49.57	3.15	48.40	3.24	47.23	3.25	46.13	3.38	45.07	3.47	44.03	3.49
Tc-like	52.64	1.80	51.26	1.92	49.95	2.06	48.70	2.16	47.49	2.21	46.38	2.49	45.29	2.60	44.24	2.75	43.24	2.97
Ru-like	51.94	1.51	50.56	1.51	49.24	1.54	48.01	1.86	46.83	2.05	45.69	2.12	44.60	2.32	43.56	2.50	42.53	2.44
Rh-like	51.23	0.58	49.85	0.56	48.57	1.33	47.33	1.34	46.13	1.34	45.02	1.77	43.95	2.03	42.90	2.05	41.95	2.62
Pd-like	50.56	0.00	49.19	0.00	47.89	0.00	46.74	2.13	45.56	2.18	44.44	2.23	43.36	2.28	42.33	2.33	41.34	2.38

Table 3. Calculated mean wavelength $\bar{\lambda}_{gA}$ and spectral width $\Delta\lambda_{gA}$ for the configuration interaction unresolved transition arrays of thallium through actinium ions: Rb-like to Rh-like ions for the 4p - 4d arrays and Rb-like to Pd-like ions for the 4d - 4f arrays. Wavelengths throughout the table are given in $\mathring{A}$.

4p - 4d	Tl		Pb		Bi		Po		At		Rn		Fr		Ra		Ac	
Ion	$\bar{\lambda}_{gA}$	$\Delta\lambda_{gA}$	$\bar{\lambda}_{gA}$	$\Delta\lambda_{gA}$	$\bar{\lambda}_{gA}$	$\Delta\lambda_{gA}$	$\bar{\lambda}_{gA}$	$\Delta\lambda_{gA}$	$\bar{\lambda}_{gA}$	$\Delta\lambda_{gA}$	$\bar{\lambda}_{gA}$	$\Delta\lambda_{gA}$	$\bar{\lambda}_{gA}$	$\Delta\lambda_{gA}$	$\bar{\lambda}_{gA}$	$\Delta\lambda_{gA}$	$\bar{\lambda}_{gA}$	$\Delta\lambda_{gA}$
Rb-like	36.90	10.93	35.54	10.85	34.20	10.71	32.92	10.58	32.30	12.09	31.08	11.91	29.91	11.72	28.76	11.50	27.66	11.28
Sr-like	36.36	9.21	35.09	9.40	33.68	9.06	32.61	9.58	31.42	9.52	30.19	9.29	29.16	9.49	28.26	9.93	27.18	9.74
Y-like	35.59	6.08	34.35	6.51	33.19	7.16	31.90	6.93	30.67	6.85	29.54	6.98	28.63	7.69	27.80	8.42	26.65	8.09
Zr-like	35.35	5.12	34.14	5.61	32.77	5.21	31.58	5.49	30.44	5.70	29.43	6.28	28.36	6.42	27.58	7.34	26.35	6.77
Nb-like	35.08	3.62	33.78	3.73	32.44	3.22	31.29	3.83	30.24	4.69	29.06	4.55	28.06	5.04	26.90	4.58	36.06	5.50
Mo-like	34.90	2.83	33.57	2.71	32.36	3.15	31.11	2.78	29.98	3.15	29.12	4.65	27.72	3.15	26.81	3.91	25.83	4.30
Tc-like	34.74	2.34	33.42	2.01	32.15	1.71	30.97	1.92	29.77	1.59	28.65	1.54	27.54	1.31	26.67	3.17	25.74	3.61
Ru-like	34.59	2.17	33.28	1.33	32.04	1.25	30.85	1.18	29.69	1.11	28.58	1.04	27.50	0.98	26.45	0.92	25.44	0.86
Rh-like	34.57	3.78	33.29	3.42	31.91	0.00	30.74	0.00	29.75	3.11	28.65	3.11	27.58	3.02	26.53	2.84	25.41	0.00

4d - 4f	Tl		Pb		Bi		Po		At		Rn		Fr		Ra		Ac	
Ion	$\bar{\lambda}_{gA}$	$\Delta\lambda_{gA}$	$\bar{\lambda}_{gA}$	$\Delta\lambda_{gA}$	$\bar{\lambda}_{gA}$	$\Delta\lambda_{gA}$	$\bar{\lambda}_{gA}$	$\Delta\lambda_{gA}$	$\bar{\lambda}_{gA}$	$\Delta\lambda_{gA}$	$\bar{\lambda}_{gA}$	$\Delta\lambda_{gA}$	$\bar{\lambda}_{gA}$	$\Delta\lambda_{gA}$	$\bar{\lambda}_{gA}$	$\Delta\lambda_{gA}$	$\bar{\lambda}_{gA}$	$\Delta\lambda_{gA}$
Rb-like	48.65	5.43	47.43	5.38	46.24	5.29	45.13	5.24	42.29	0.00	41.26	0.00	40.27	0.00	39.31	0.00	38.38	0.00
Sr-like	47.39	5.99	46.24	5.84	45.16	5.79	43.92	5.60	42.97	5.66	41.97	5.49	40.87	5.30	39.85	4.76	38.83	4.74
Y-like	46.51	6.01	45.41	5.84	44.20	5.63	43.24	5.54	42.17	5.40	41.15	5.27	40.09	5.02	39.09	4.80	38.12	4.60
Zr-like	45.03	5.02	44.01	4.94	43.06	5.04	42.07	5.05	41.10	4.94	40.18	4.86	39.29	4.82	38.44	4.78	37.55	4.72
Nb-like	43.97	4.31	42.99	4.39	42.04	4.44	41.10	4.41	40.16	4.31	39.28	4.33	38.43	4.34	37.60	4.35	36.74	4.22
Mo-like	43.03	3.56	42.05	3.56	41.10	3.56	40.22	3.69	39.34	3.73	38.48	3.75	37.65	3.80	36.86	3.87	36.06	3.85
Tc-like	42.23	2.92	41.29	3.05	40.37	3.08	39.48	3.10	38.63	3.21	37.84	3.50	37.01	3.46	36.23	3.54	35.46	3.54
Ru-like	41.57	2.62	40.64	2.74	39.74	2.87	38.87	2.95	38.02	3.00	37.20	3.06	36.42	3.16	35.66	3.28	34.92	3.35
Rh-like	40.95	2.34	40.04	2.57	39.19	2.91	38.33	2.98	37.50	3.04	36.69	3.09	35.91	3.14	35.15	3.19	34.42	3.22
Pd-like	40.39	2.43	39.47	2.48	38.59	2.54	37.74	2.59	36.92	2.64	36.12	2.69	35.35	2.74	34.61	2.78	33.89	2.83